
Figures and figure supplements

Structural characterization of NrnC identifies unifying features of dinucleases

Justin D Lormand et al

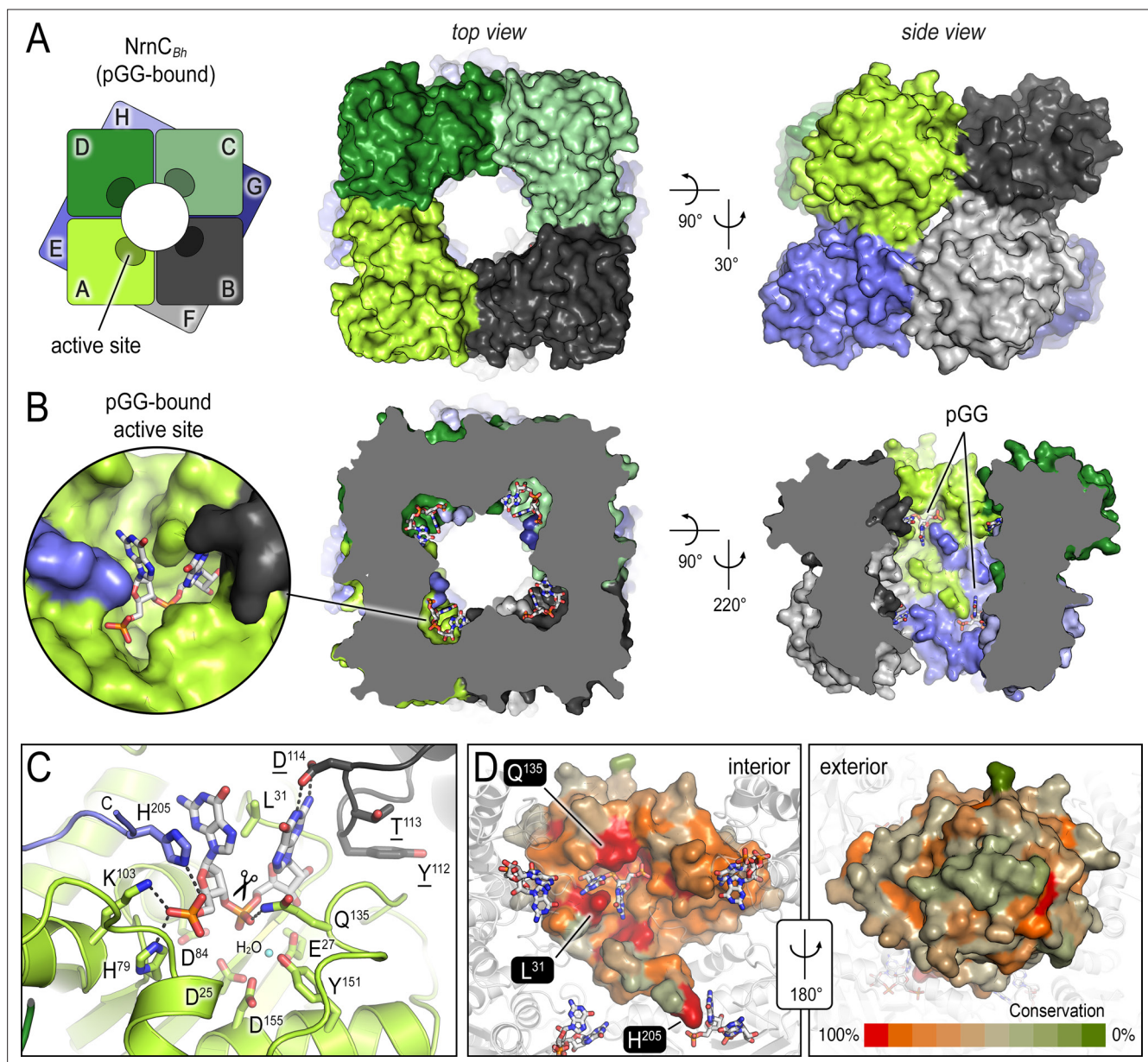


Figure 1. The crystal structures of *B. henselae* nano-RNase C (NrnC) bound to pGG reveals motifs defining substrate specificity. **(A)** The octameric assembly. NrnC_{Bh} is shown as surface representation in two views. Each monomer is shown in a distinct color. The cartoon illustrates the stacking of the two tetrameric NrnC rings that form the octamer with a central, round opening. **(B)** Active-site position. Each monomer contributes one active site, here bound to the substrate pGG, facing toward NrnC's central pore. Each active site includes a C-terminal tail of a subunit from an adjacent ring. **(C)** Substrate coordination. The catalytic DEDDY motif and residues coordinating each moiety of pGG contacts are shown as sticks, with carbon residues colored according to monomer identity. Residue Y¹⁵¹ coordinates water molecule near the scissile bond. **(D)** Conservation mapping on a surface representation of a NrnC monomer. Conservation scores were calculated based on a multisequence alignments (MUSCLE; [Edgar, 2004](#)) of NrnC homologs identified using a sequence search on the EggNOG resource, version 5.0.0 ([Huerta-Cepas et al., 2019](#)) and the sequence of NrnC_{Bh} as the input. Outliers were identified based on sequence length and non-consensus insertions, resulting in a final collection of 560 sequences of putative NrnC orthologs. The two views, separated by a 180° rotation, show the cavity-facing (interior, left) and outer-facing (exterior, right) surface regions.

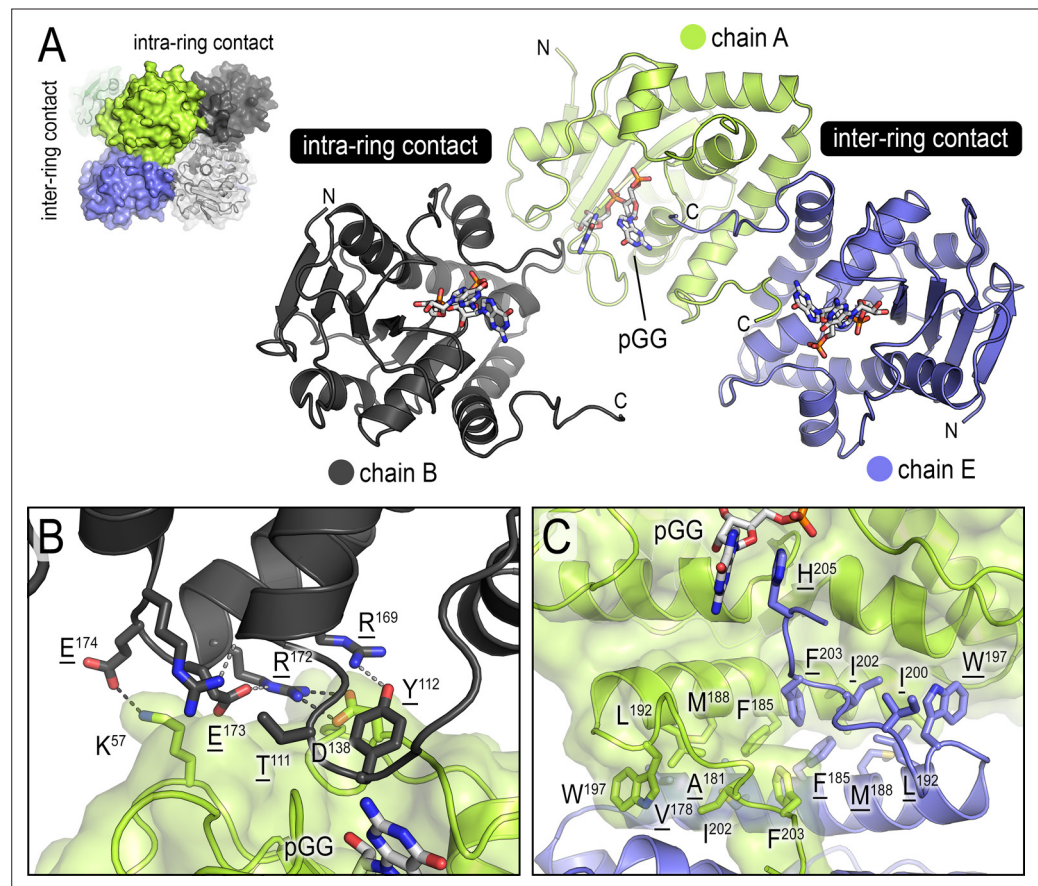


Figure 1—figure supplement 1. Inter- and intra-ring contacts in the NrnC_{Bh} octamer. (A) Overview of three pGG-bound NrnC_{Bh} monomers. The monomers are shown in cartoon representation. The chain colored in dark gray forms an intra-ring contact with the central, green-colored chain, whereas the chain colored in blue forms a representative inter-ring contact within the octameric nano-RNase C (NrnC). (B) Detailed intra-ring interface. (C) Detailed inter-ring interface. Residues contributing direct interactions between monomers are shown as sticks. Representative hydrogen bonds are shown as dashed lines.

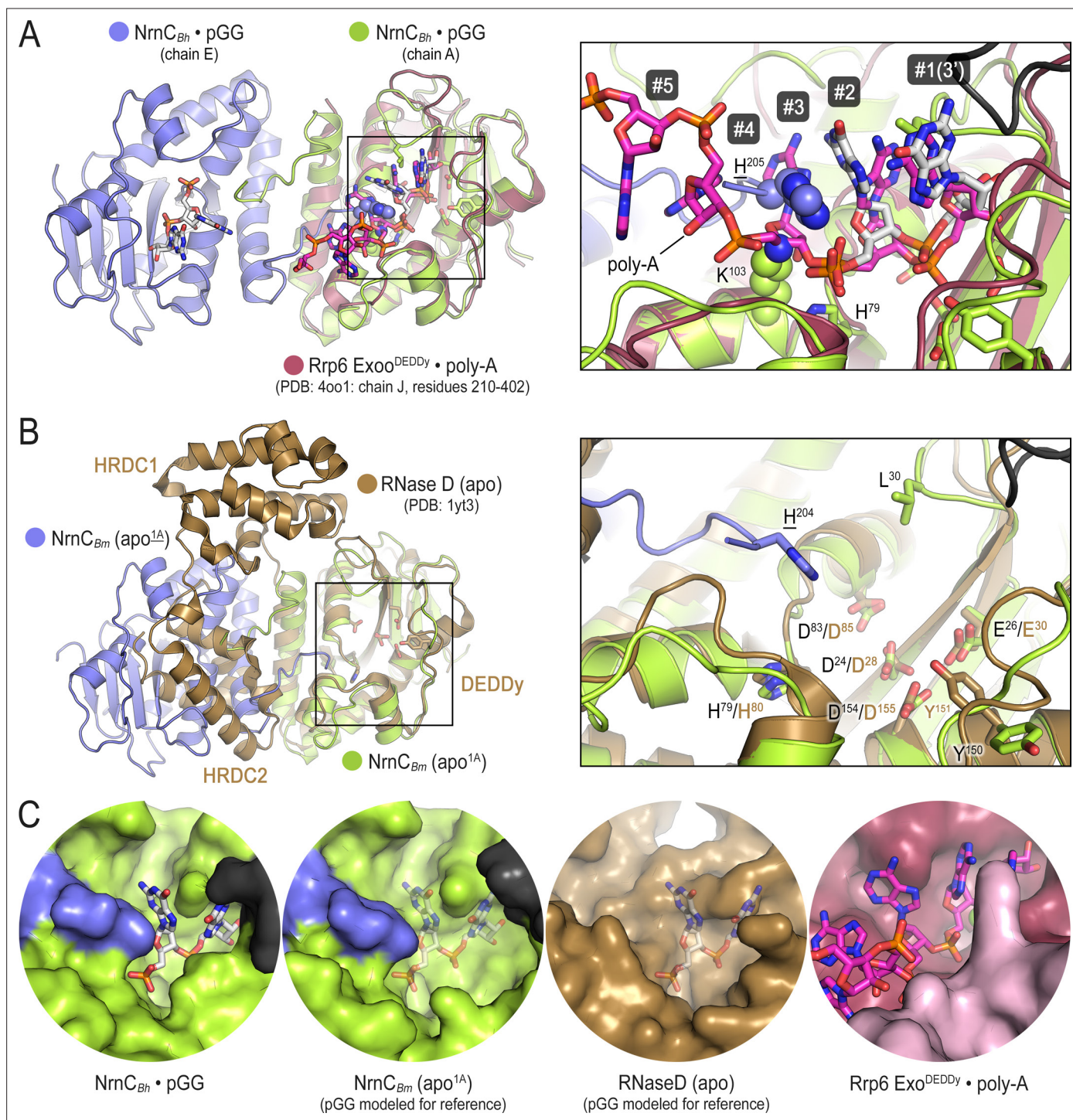


Figure 1—figure supplement 2. Comparison of nano-RNase C (NrnC) to structurally related proteins reveals the constricted nature of NrnC's active site. **(A)** A pGG-bound NrnC_{Bh} inter-ring dimer (slate and green chains, with pGG carbon atoms shown in white) was superimposed on a structure of the exosome's Rrp6 exonuclease (purple chain) bound to poly-A (pink carbon atoms; PDB:4oo1; *Wasmuth et al., 2014*). The inset shows a detailed view of the superimposed active sites. Numbering refers to the residues in the substrate. Phosphate cap residues of NrnC that block the path of poly-A substrate are shown as spheres. The black protein chain in top-right corner stems from an adjacent intra-ring monomer. **(B)** A substrate-free NrnC_{Bm} inter-ring dimer (slate and green chains) was superimposed on a structure of apo-RNase D (*Zuo et al., 2005*), highlighting conservation of the catalytic DEDDy motif and differences in regions around NrnC's L-wedge and phosphate cap (inset). **(C)** Surface views of the active sites of NrnC, RNaseD, and Rrp6 accentuate the constraint of the NrnC active site. Translucent pGG represents modeled substrate as opposed to co-crystallized substrate.

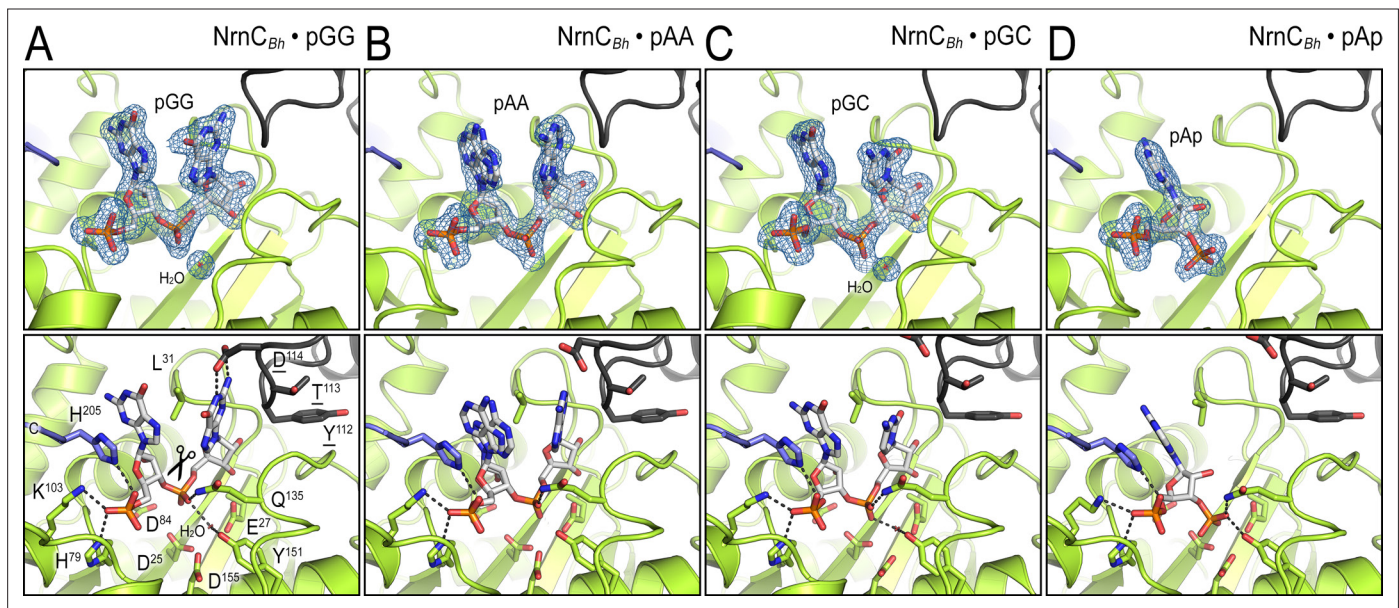


Figure 1—figure supplement 3. Structural comparison of NrnC_{Bh} bound to various ribonucleotides. **(A)** Diribonucleotide pGG-bound NrnC_{Bh}, identical to the structure shown in **Figure 1**. **(B)** Diribonucleotide pAA-bound NrnC_{Bh}. **(C)** Diribonucleotide pGC-bound NrnC_{Bh}. **(D)** Adenosine-3',5'-bisphosphate (pAp)-bound NrnC_{Bh}. The top row of images shows nano-RNase C (NrnC) as a cartoon representation with the nucleotide substrate represented as sticks with carbon atoms colored white. Polder omit maps for each substrate are shown as blue mesh. The bottom row shows detailed views of the active site residues contacting each ribonucleotide.

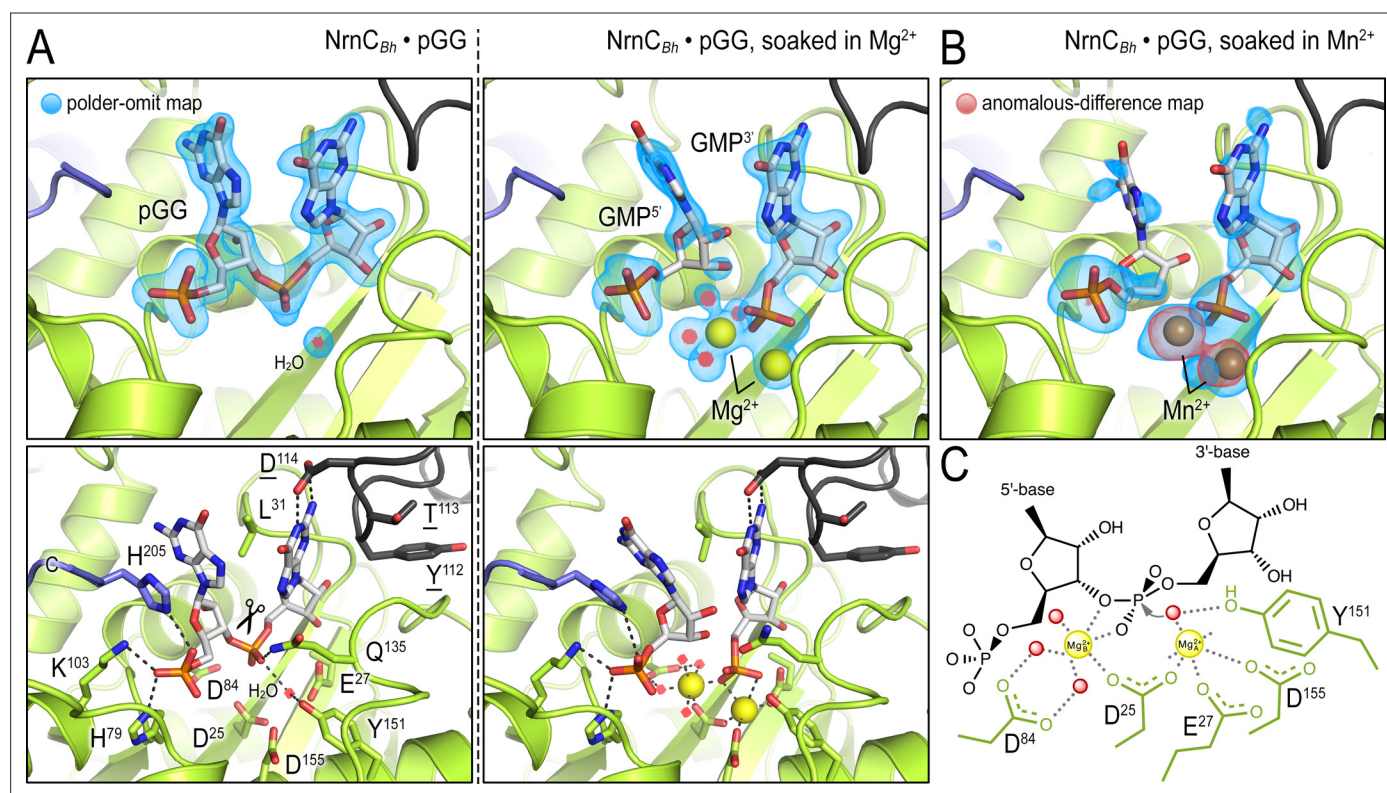


Figure 1—figure supplement 4. *In crystallo* catalysis indicates a two-metal mechanism of NrnC_{Bh} activity. **(A)** Active sites of NrnC_{Bh}•pGG, before and after soaking crystals in a solution containing Mg²⁺ prior to data collection. **(B)** Active site of NrnC_{Bh}•pGG, after soaking crystals in a solution containing Mn²⁺ prior to data collection. Top panels show polder omit maps highlighting nucleotide and metal density. The red density in **(B)** represents an anomalous-difference map calculated from data collected at the Mn²⁺ absorption edge. The bottom panels show specific active site contacts between protein, nucleotide, ions, and water molecules. **(C)** Schematic overview of two-metal coordination at the active site of nano-RNase C (NrnC).

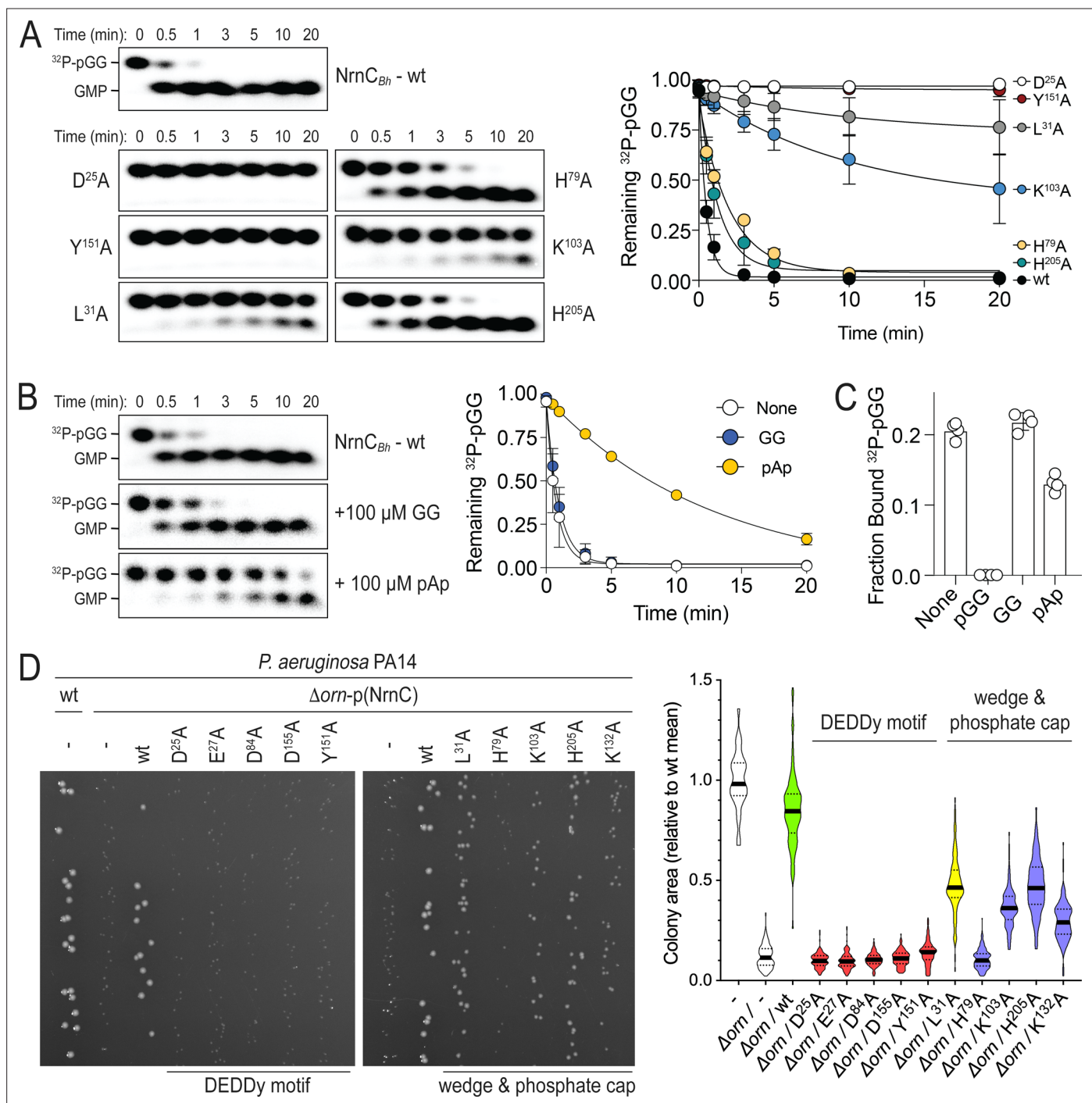


Figure 2. Phosphate cap and L-wedge contribute to nano-RNase C's (NrnC's) diribonuclease activity. **(A)** In vitro enzyme activity. Degradation of ^{32}P -pGG (1 μM total) by purified wild-type NrnC_{Bh} or variants with alanine substitutions (5 nM) at the indicated sites was assessed. Samples were stopped at the indicated times (min) and analyzed by denaturing 20% PAGE. Representative gels are shown (left). The graph (right) shows the means and SD of three independent experiments. **(B)** Effect of a dinucleotide lacking the 5' phosphate (GG) and pAp on NrnC catalysis. pGG processing was assessed as in **(A)** but in the presence or absence of 100-fold excess (over ^{32}P -pGG) GpG or pAp. Representative gels (left) and quantification from three independent experiments (right) are shown. Means and SD are plotted. **(C)** Competition binding studies. Fraction bound of ^{32}P -pGpG to 200 nM purified NrnC_{Bh} in the presence of no competitor, 100 μM pGG, 100 μM GpG, or 100 μM pAp is plotted as individual data, means, and SD of four independent experiments. **(D)** Complementation of the small-colony phenotype of *P. aeruginosa* Δorn by wild-type and mutant NrnC_{Bh}. Bacterial cultures were diluted and dripped on LB agar plates. After overnight incubation, representative images of the plates were taken (left). Experiments were performed in triplicate. Quantification of respective colony sizes is shown as violin plots (right).

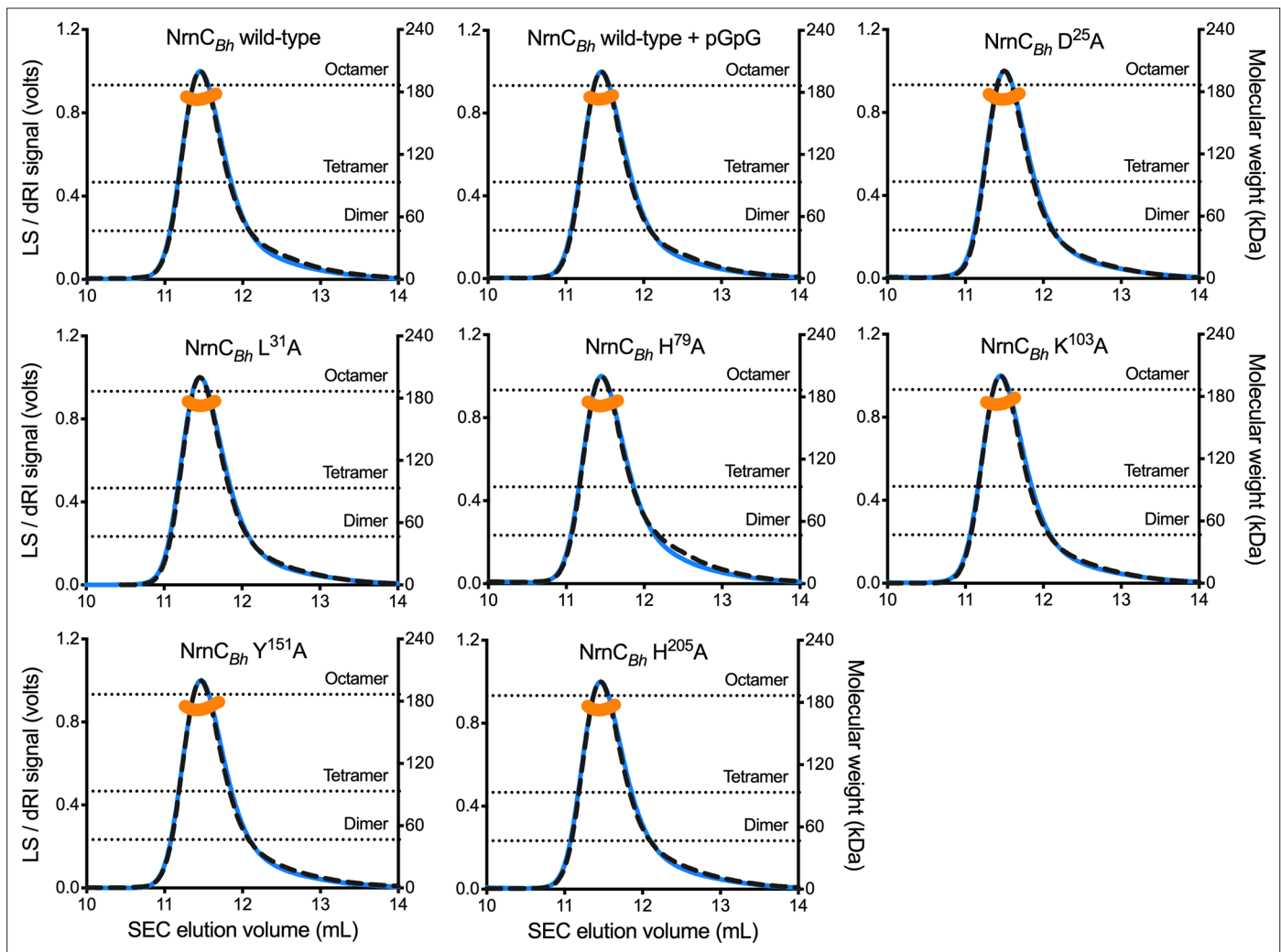


Figure 2—figure supplement 1. SEC-MALS of *NrnC_{Bh}* wild-type and mutant variants. Molecular weight determination indicates that pGpG binding does not impact oligomerization, and that purified *NrnC_{Bh}* point mutants remain octameric in solution. Absolute molecular weights of nano-RNase C (*NrnC*) are shown as orange data points across elution peaks plotted on the right axis. Theoretical oligomerization states are shown as dashed horizontal lines. 90°-light scattering: blue solid lines; refractive index signal: black dashed lines; plotted on left axis.

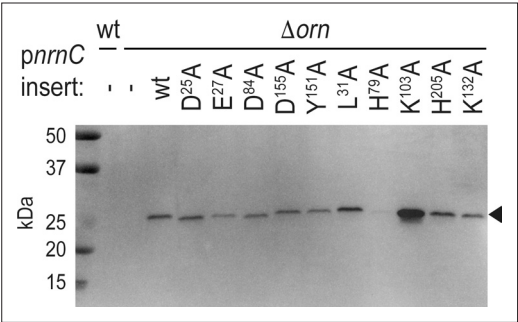


Figure 2—figure supplement 2. Expression of NrnC_{BH} wild-type and mutant variants in *P. aeruginosa* Δ*orn*. Cell lysates were analyzed by western blotting, detecting the C-terminal HA-tag in recombinantly expressed NrnC_{BH}.

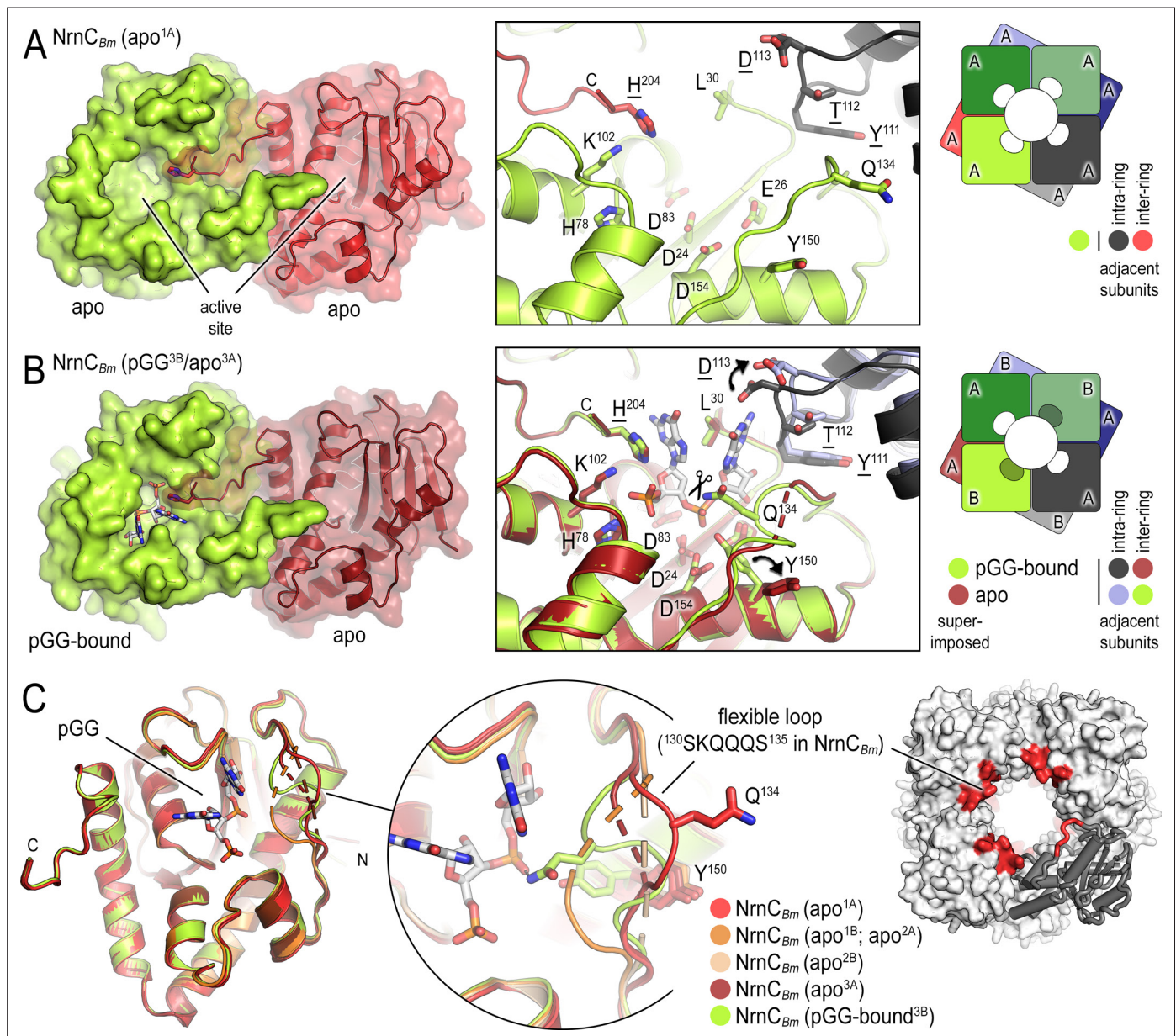


Figure 3. *B. melitensis* nano-RNase C (NrnC) crystal structures reveal a flexible loop that constraints the enzyme's active site. **(A)** Crystal structure of apo-NrnC_{Bm}. A crystallographic dimer as part of the octameric assembly is shown as surface presentation (left) and close-up of the active site (middle). The diagram (right) depicts the octamer and the spatial relationship of the monomers shown. **(B)** Crystal structure of NrnC_{Bm} with alternating substrate-bound and empty active sites. The close-up (middle) shows a superposition of the two monomers in the asymmetric unit, depicting their conformational difference and adjacent monomers, with intra- and inter-ring neighbors colored as shown in the diagram (right). **(C)** Superposition of four apo-NrnC_{Bm} conformations based on three independent crystal forms (comprising chains apo^{1A}/apo^{1B} for form 1; apo^{2A}/apo^{2B} for form 2, and apo^{3A}/pGG-bound^{3B} for form 3), compared to the pGG-bound conformation of the same protein shown in **(B)**. The position of the flexible loop (red) in the NrnC octamer is shown (right panel).

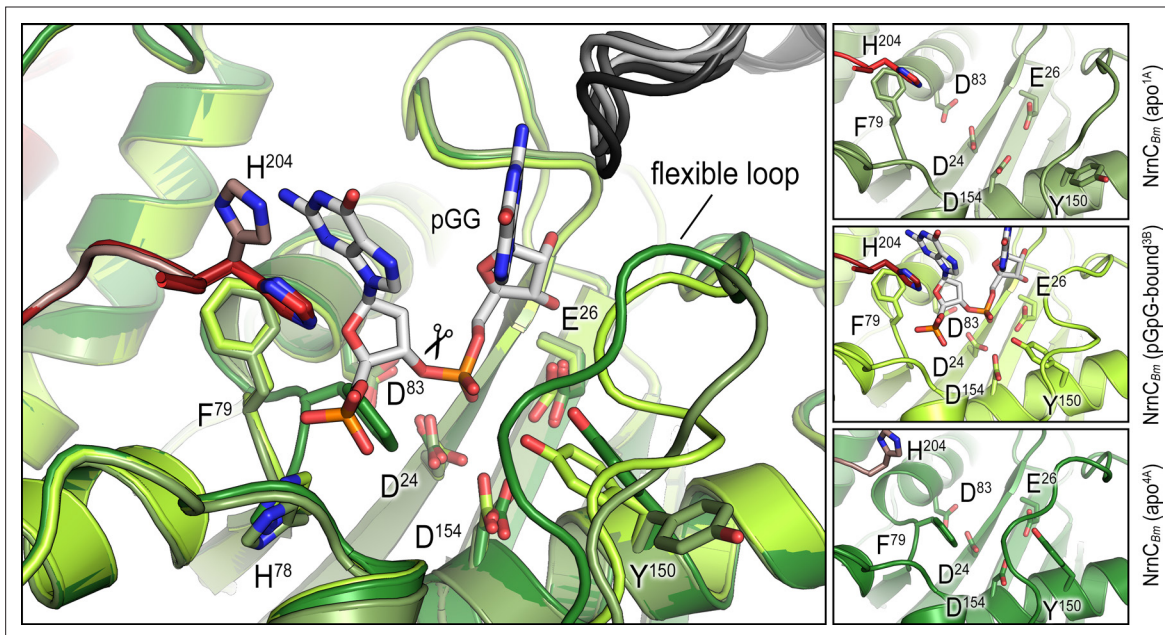


Figure 3—figure supplement 1. Overlay of an alternative crystallographic apo-NrnC_{bm} state with the apo- and pGG-bound states observed in the crystal structure shown in **Figure 3B**. The large panel shows three structures superimposed. The smaller panels on the right show each active site isolated with residues of interest labeled and shown as sticks.

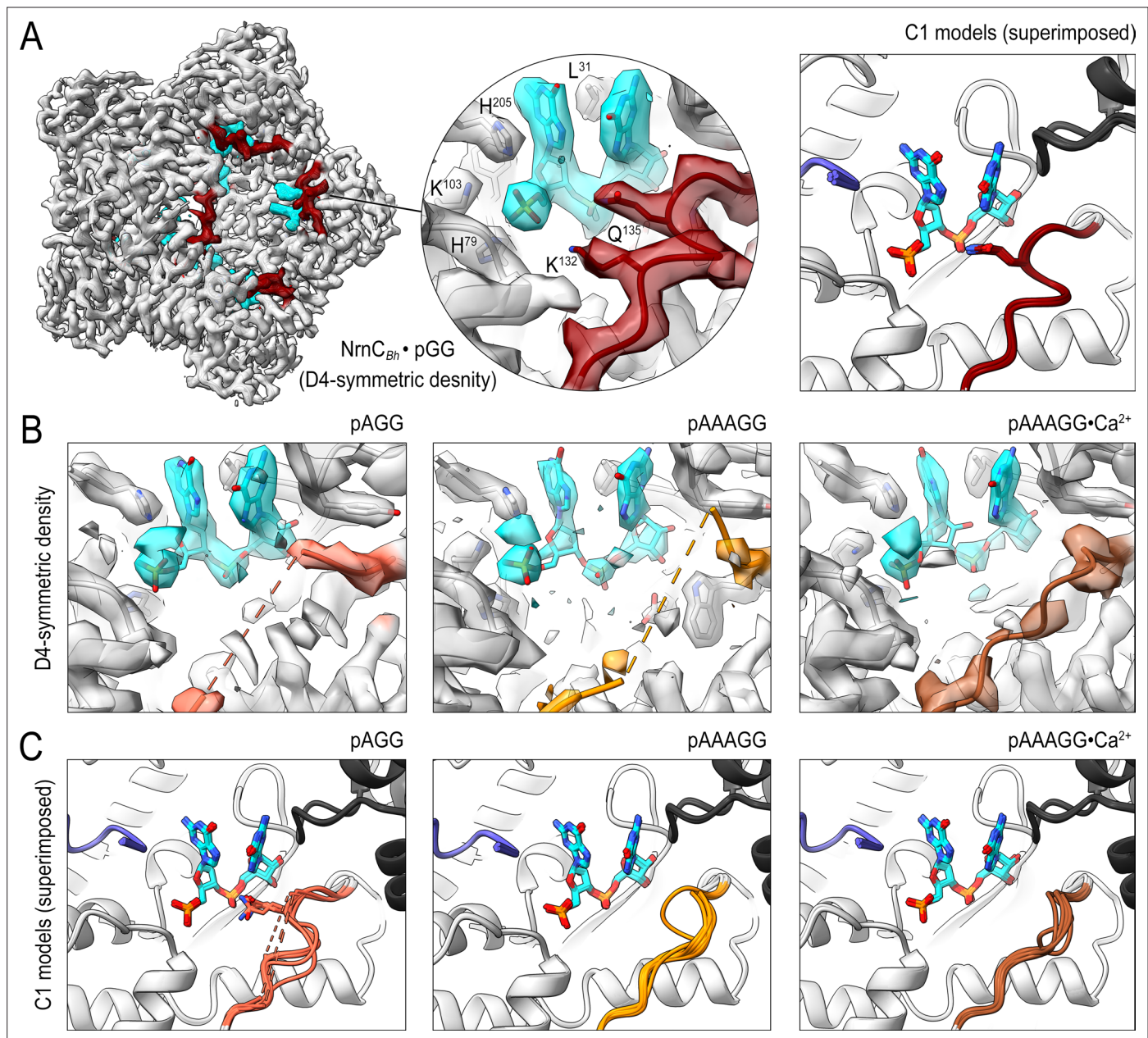


Figure 4. Cryo-electron microscopy (cryo-EM) structures of NrnC_{Bh} with 2-, 3-, 5-mer RNA substrates show substrate length-dependent active site conformations. **(A)** Electron density map of a NrnC_{Bh} octamer in complex with pGG. D4 symmetry was applied during final map refinement. pGG molecule and density are colored cyan. The SKQQQS-containing loops (residues 130–137) are colored maroon. Superposition of all eight active sites from a reconstruction with C1 symmetry (right panel) shows consensus order in the loop when bound to pGG. **(B)** Active site images shown for NrnC_{Bh} incubated with 3-mer and 5-mer (with or without Ca²⁺) RNA substrates. Regions corresponding to those shown in **(A)** are shown in color, with light red (left panel), orange (middle panel), and brown (right panel) depicting the loop/loop density from structures determined with added pAGG, pAAAGG, and pAAAGG•Ca²⁺, respectively. D4-symmetric maps are shown. **(C)** Superposition of all eight active sites from octamer reconstructions based on respective C1-symmetric maps for each RNA substrate. Color scheme is as described in **(B)**.

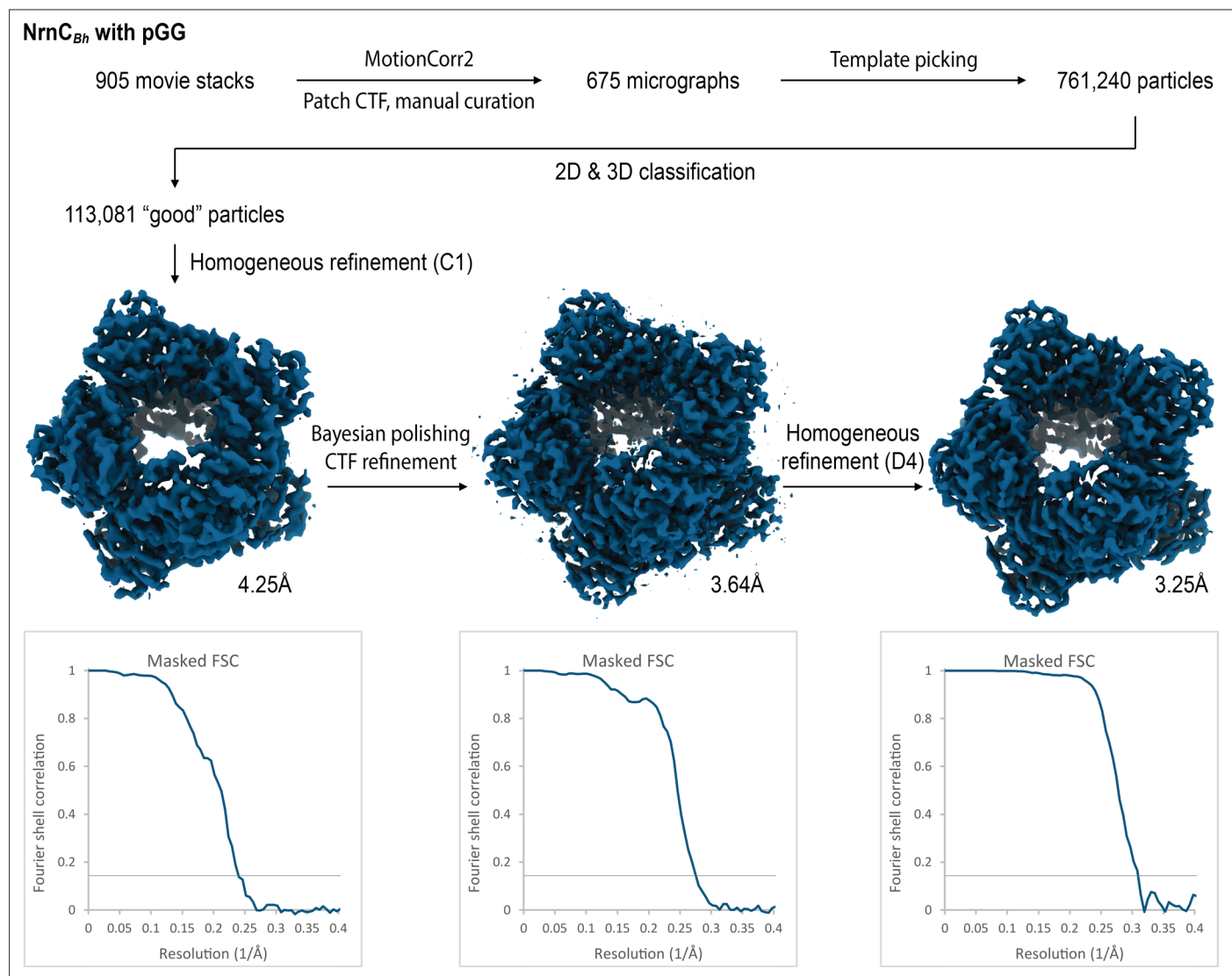


Figure 4—figure supplement 1. Cryo-electron microscopy (cryo-EM) workflow and resolution for NrnC_{Bh}•pGG.

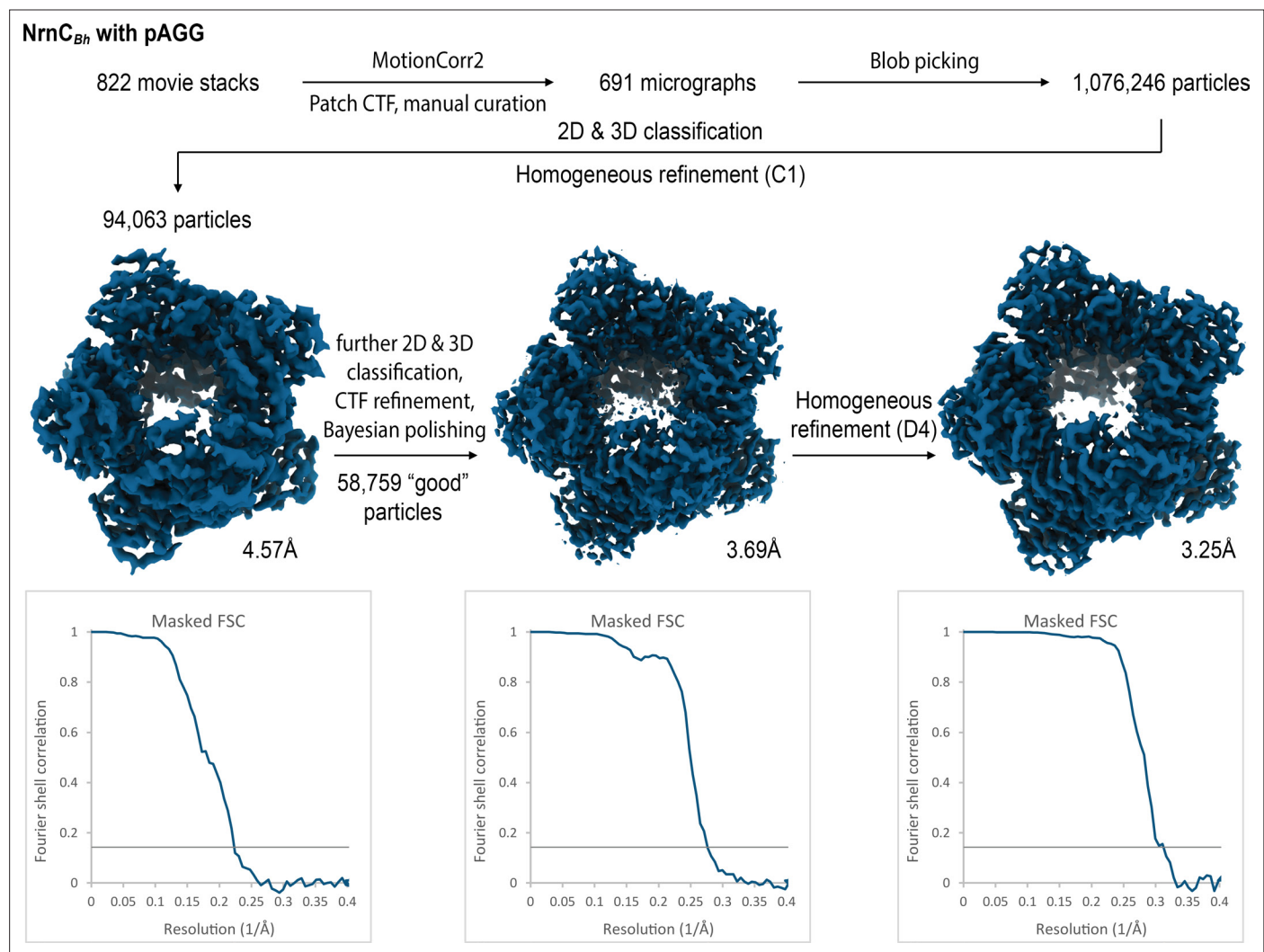


Figure 4—figure supplement 2. Cryo-electron microscopy (cryo-EM) workflow and resolution for NrnC_{Bh}•pAGG.

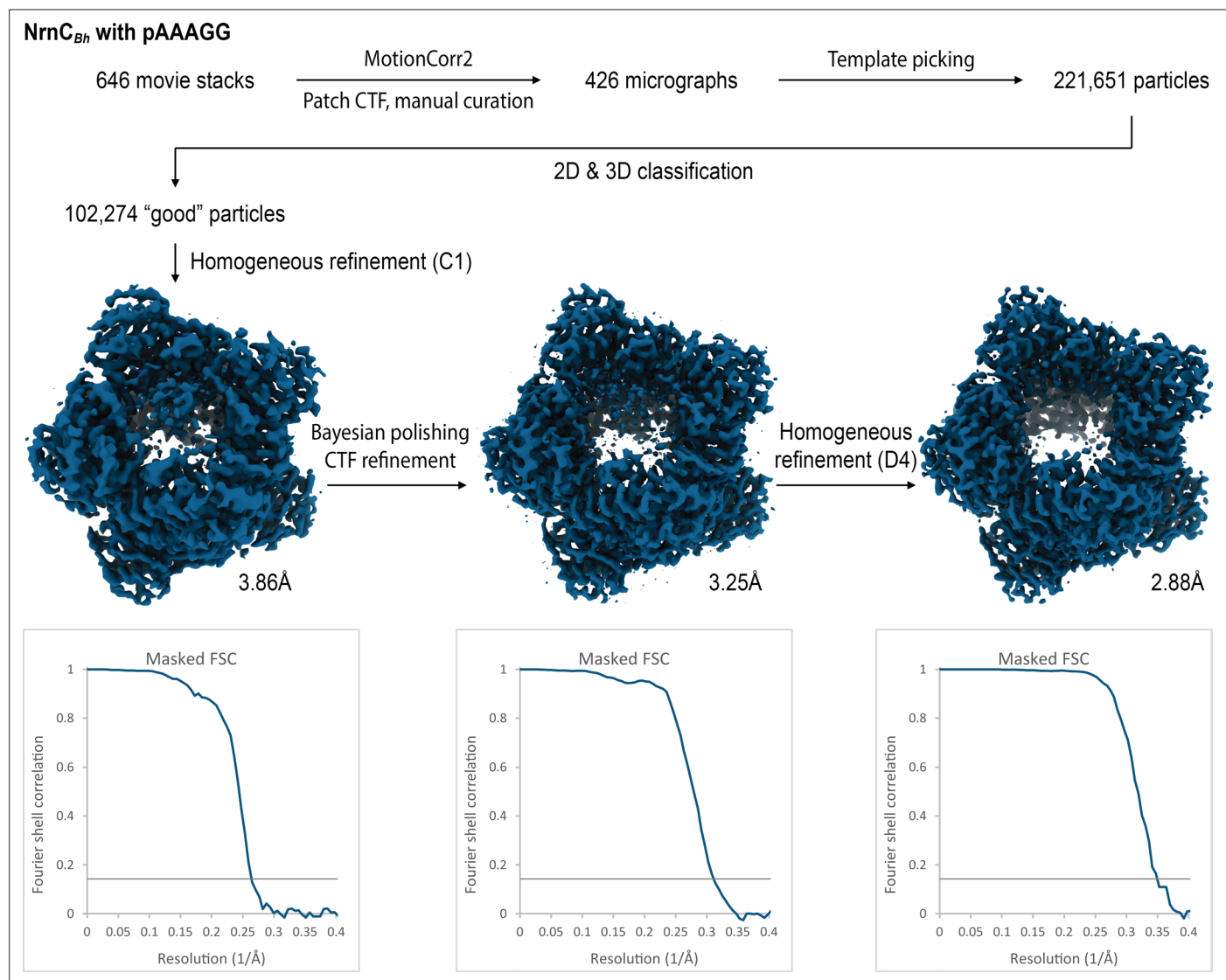


Figure 4—figure supplement 3. Cryo-electron microscopy (cryo-EM) workflow and resolution for NrnC_{Bh}•pAAAGG.

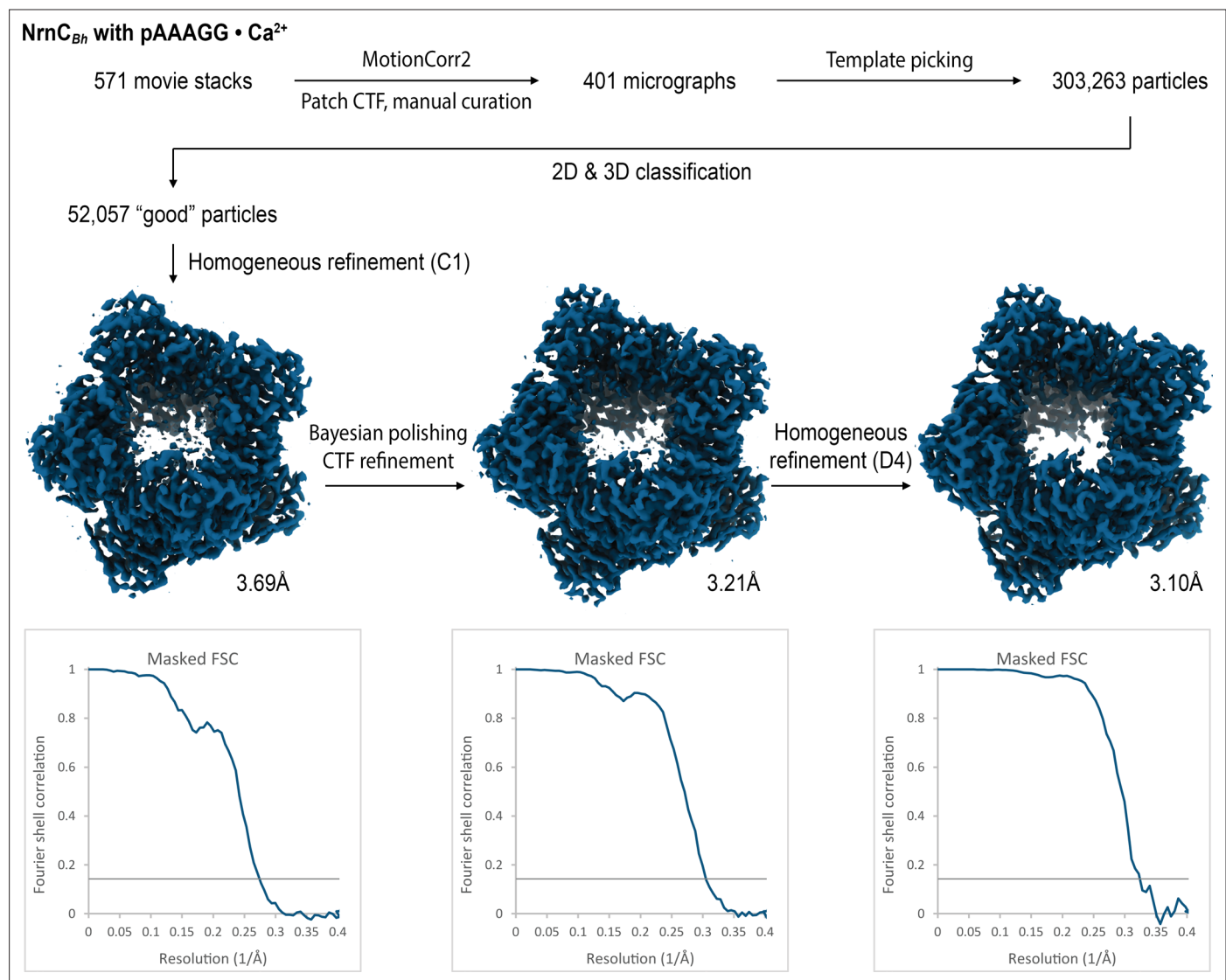


Figure 4—figure supplement 4. Cryo-electron microscopy (cryo-EM) workflow and resolution for NrnC_{Bh}•pAAAGG in the presence of Ca²⁺ ions.

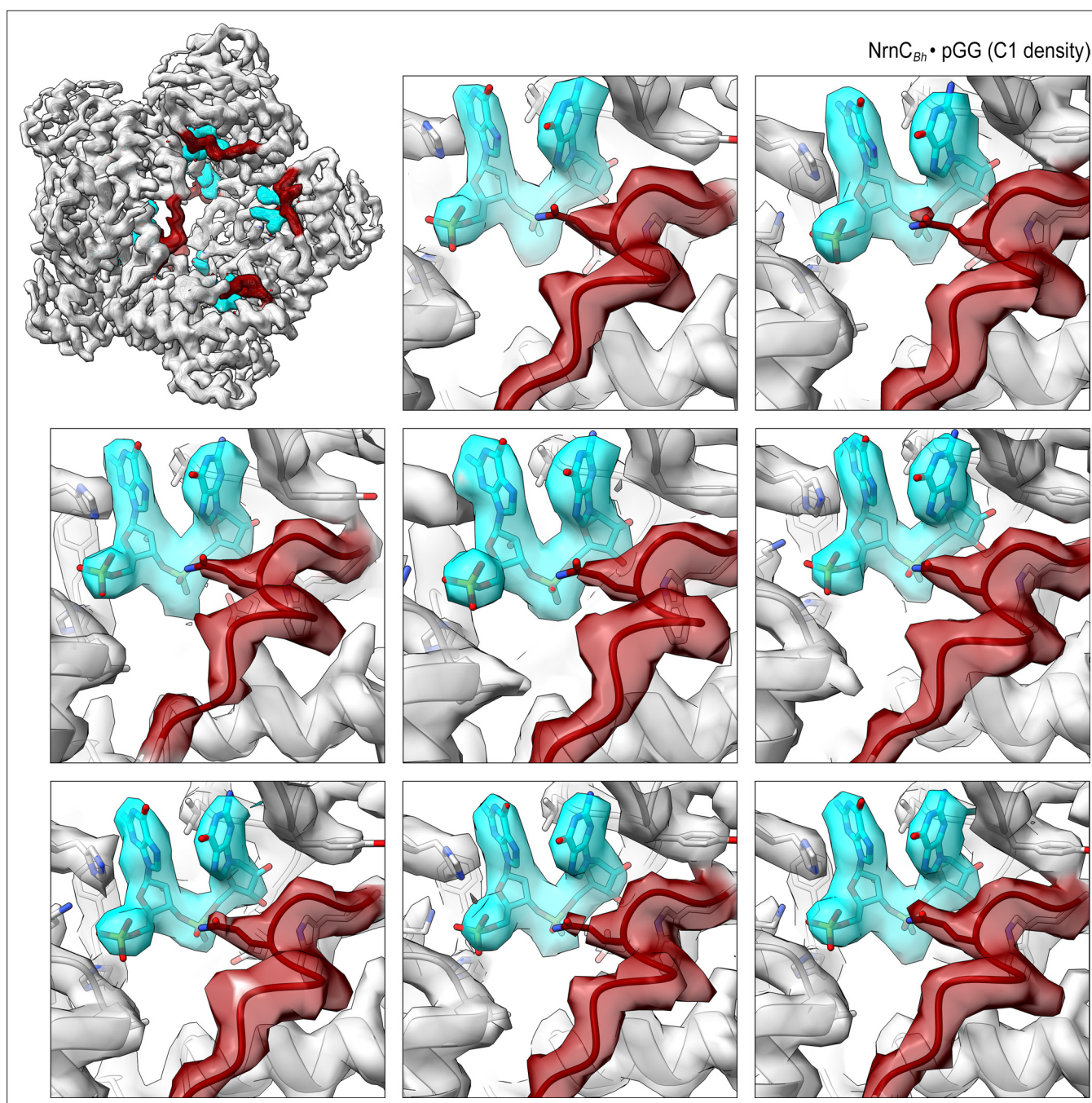


Figure 4—figure supplement 5. Overall and individual active site electron density of a NrnC_{Bh}•pGG octamer after refinement with C1 symmetry.

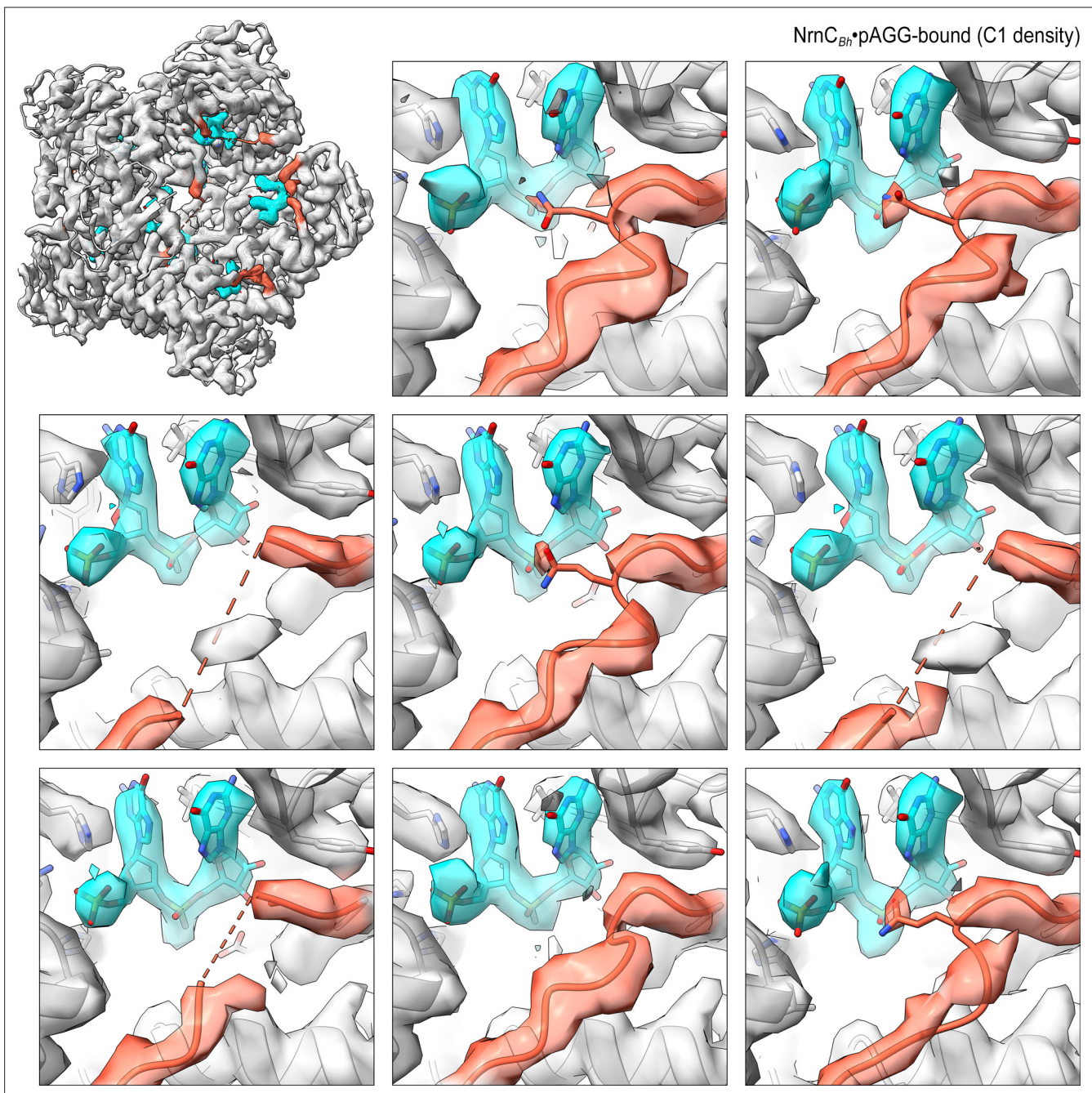


Figure 4—figure supplement 6. Overall and individual active site electron density of a NrnC_{Bh}•pAGG octamer after refinement with C1 symmetry.

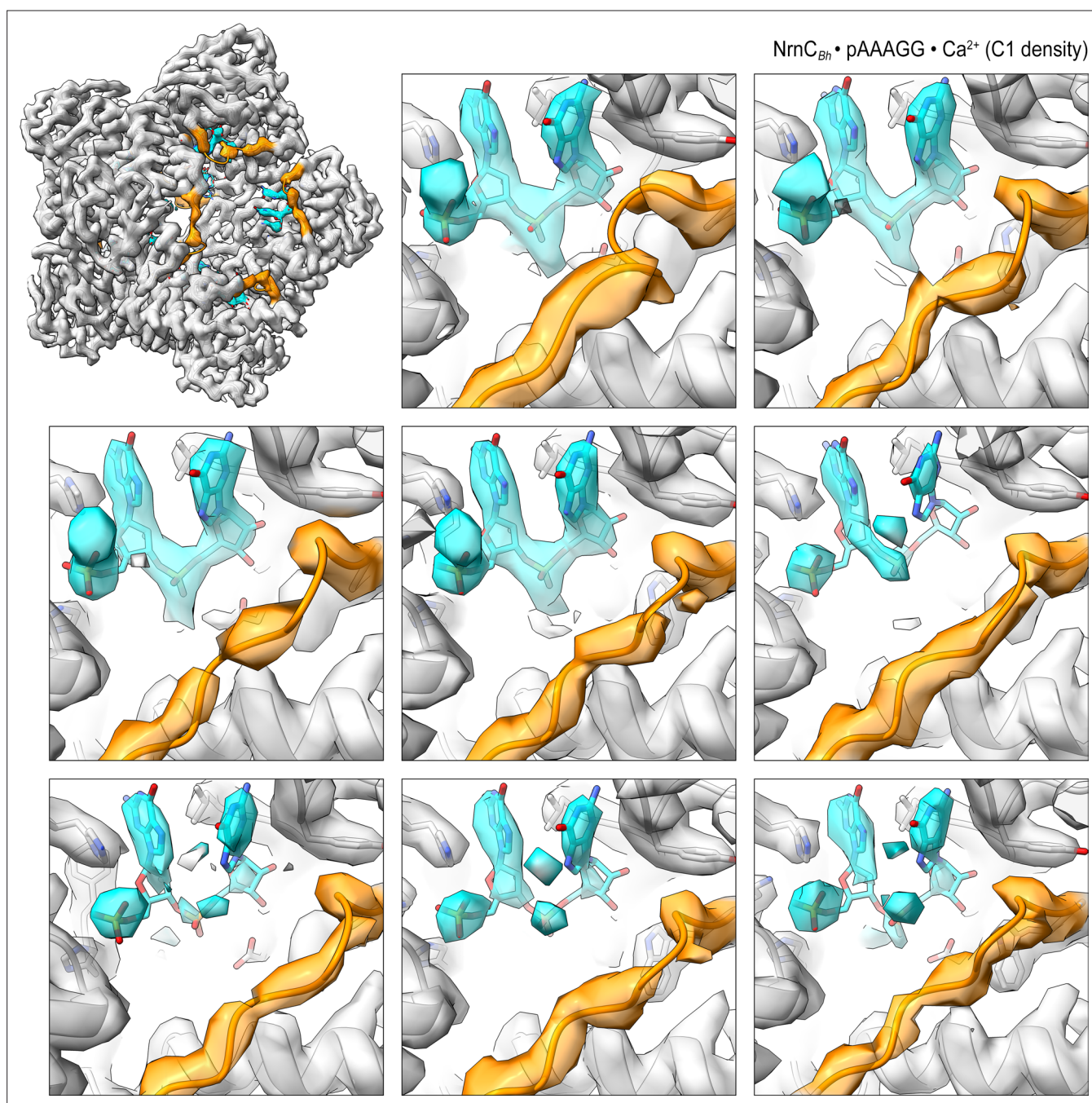


Figure 4—figure supplement 7. Overall and individual active site electron density of a NrnC_{Bh} • pAAAGG octamer after refinement with C1 symmetry.

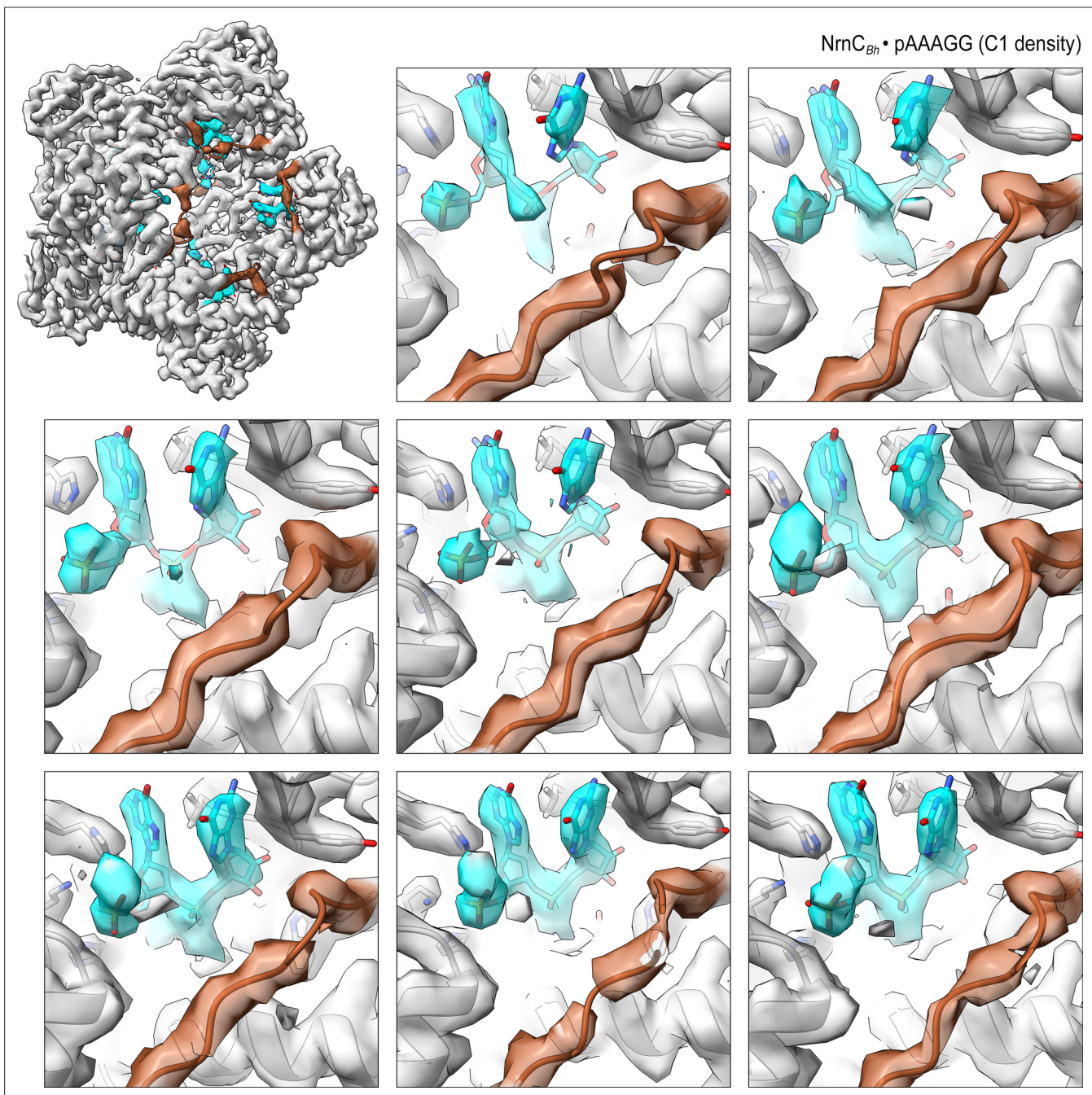


Figure 4—figure supplement 8. Overall and individual active site electron density of a $\text{NrnC}_{\text{Bh}} \cdot \text{pAAAGG}$ octamer in the presence of Ca^{2+} ions after refinement with C1 symmetry.

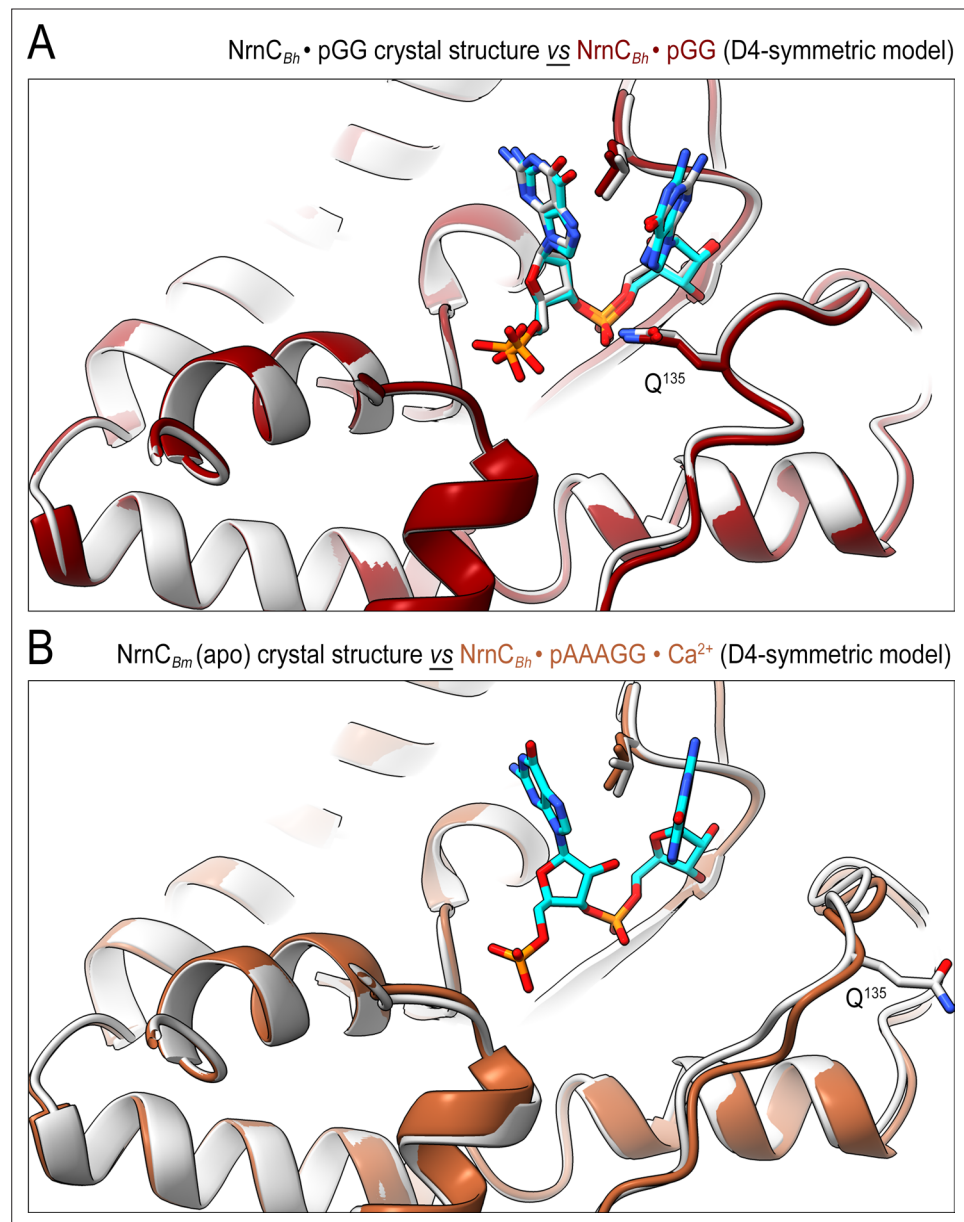


Figure 4—figure supplement 9. The conformation of nano-RNase C (NrnC) bound to substrates with more than two bases resembles the crystallographic apo-state. **(A)** Comparison of the crystal structure of $\text{NrnC}_{Bh} \cdot \text{pGG}$ with the corresponding cryo-electron microscopy (cryo-EM) structure shows agreement between the solution and crystalline state of the protein with a well-ordered conformation of the loop residues 130–137 engaging the substrate. **(B)** Comparison of the crystal structure of apo- NrnC_{Bm} with the cryo-EM structure of $\text{NrnC}_{Bm} \cdot \text{pAAAGG}$. The superposition indicates that longer substrates may bind the active site but only the first full residues appear ordered, resulting in a conformation of nano-RNase C (NrnC) similar to the inactive state observed in the apo-state crystal structures.

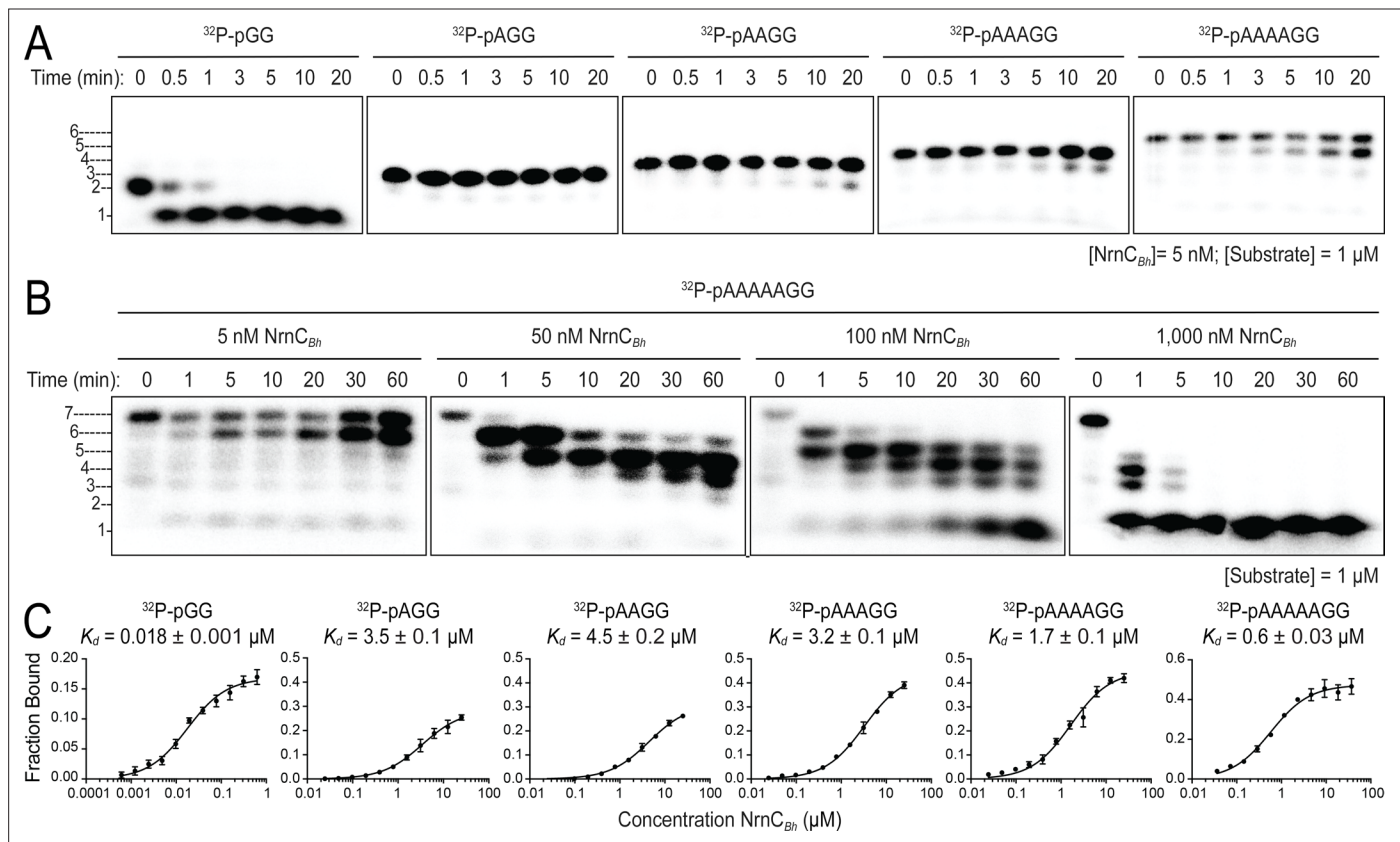


Figure 5. Nano-RNase C (NrnC) shows a strong preference for substrates with two residues in length. **(A, B)** RNase assays. Experiments are similar to those in **Figure 2** but were performed with radiolabeled substrates from 2 to 7 residues in length. Representative gels of at least two independent experiments are shown. In **(B)**, enzyme concentration was varied from 5 to 1000 nM (1:200 to 1:1 enzyme:substrate ratio). Substrate length-dependent binding studies. **(C)** Affinity of NrnC for RNA with different lengths. Fraction bound of radiolabeled substrates of increasing length was assessed at different NrnC concentrations and is plotted as means and SD from three independent experiments.

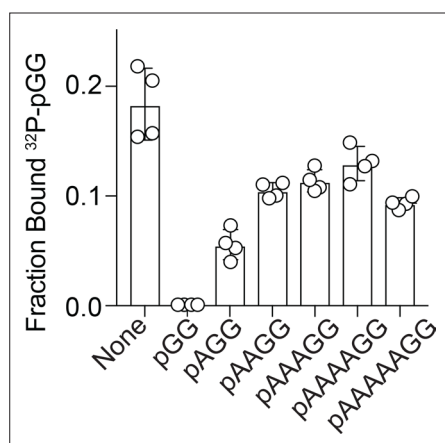


Figure 5—figure supplement 1. Competition binding studies. Fraction bound of ^{32}P -pGG to 200 nM purified NrnC_{Bh} in the presence of no competitor or 100 μM unlabeled RNA as indicated. Individual data, means, and SD of four independent experiments are plotted.

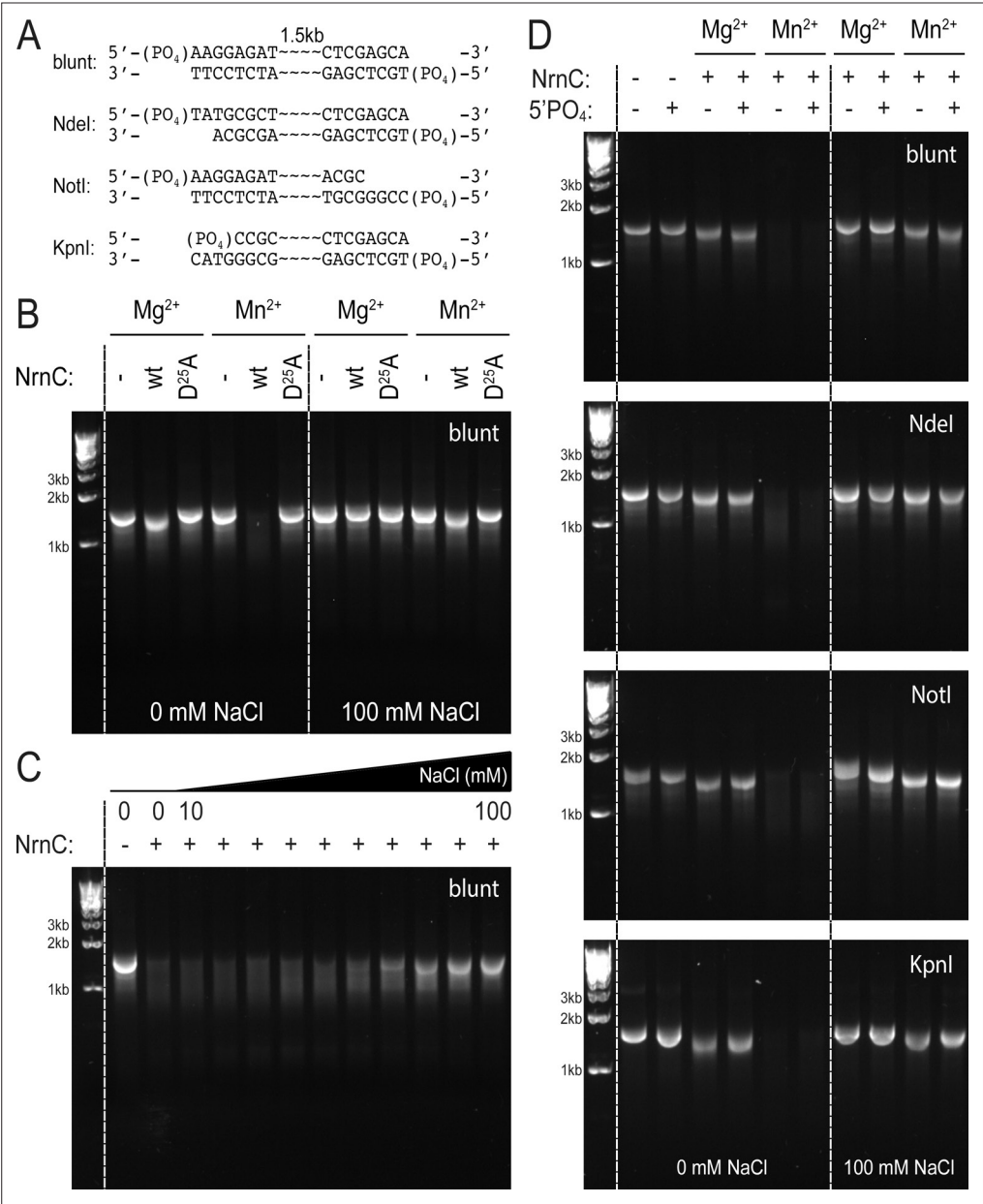


Figure 5—figure supplement 2. NrnC_{Bh} degrades long DNA fragments under distinct conditions. **(A)** DNA fragments tested in this assay. **(B)** DNase activity of wild-type NrnC_{Bh} and a catalytically inactive mutant variant on blunt dsDNA in the presence of either Mg²⁺ or Mn²⁺ and in the absence or presence of NaCl. **(C)** NaCl titration on blunt dsDNA using wild-type NrnC_{Bh}. **(D)** Nano-RNase C (NrnC) activity on various dsDNA substrates with or without a 5'-PO₄ and in the presence of Mg²⁺ of Mn²⁺. Representative agarose gels are shown from at least two independent experiments.

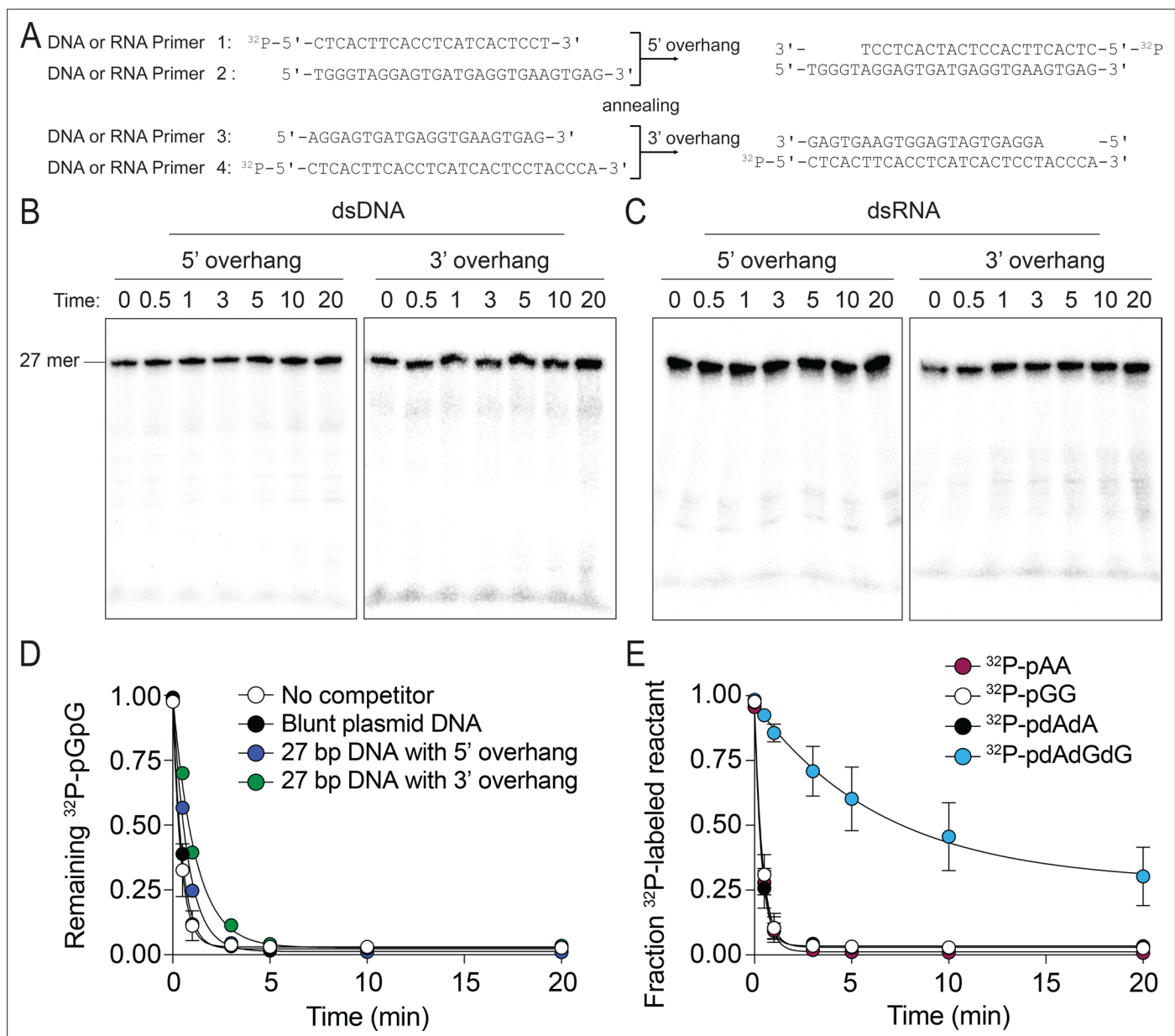


Figure 5—figure supplement 3. The preferred substrates of NrnC_{Bh} are diribonucleotides and deoxy-dinucleotides. (A–C) NrnC_{Bh} does not degrade dsDNA and dsRNA. DNA or RNA oligonucleotide sequences used are shown in (A). Primers 1 and 2 were annealed to generate a 27-nucleotide DNA or RNA with a 5' overhang and primers 3 and 4 were annealed to generate a 3' overhang (length of overhang: 5 nucleotides). NrnC_{Bh} activity on 5' overhang or 3' overhang of DNA (B) and RNA (C) in the presence of Mg^{2+} and 100 mM NaCl. These experiments were performed with 3.3 nM of 5'-radiolabeled DNA or RNA. Aliquots of each reaction were stopped at the indicated times and analyzed by 20% urea PAGE. (D) dsDNA is not an inhibitor of NrnC_{Bh} 's activity on diribonucleotides. The rate of ^{32}P -pGG degradation by 5 nM NrnC_{Bh} was assayed over time with no competitor, plasmid DNA (30 nM) that was cut with *Stu*I, or primers (1 μM) annealed to generate 5-nucleotide 5' or 3' overhangs (primers in panel A). Samples were stopped at the indicated time points and analyzed by thin-layer chromatography. Data are from triplicate independent experiments. (E) NrnC_{Bh} cleaves DNA deoxy-dinucleotides. Degradation of ^{32}P -pGG, pAA, pdAdA, and pdAdGdG (3.3 nM) by 5 nM NrnC_{Bh} is shown. Samples were stopped at the indicated time points and analyzed by TLC. The graph shows quantification of triplicate independent experiments.

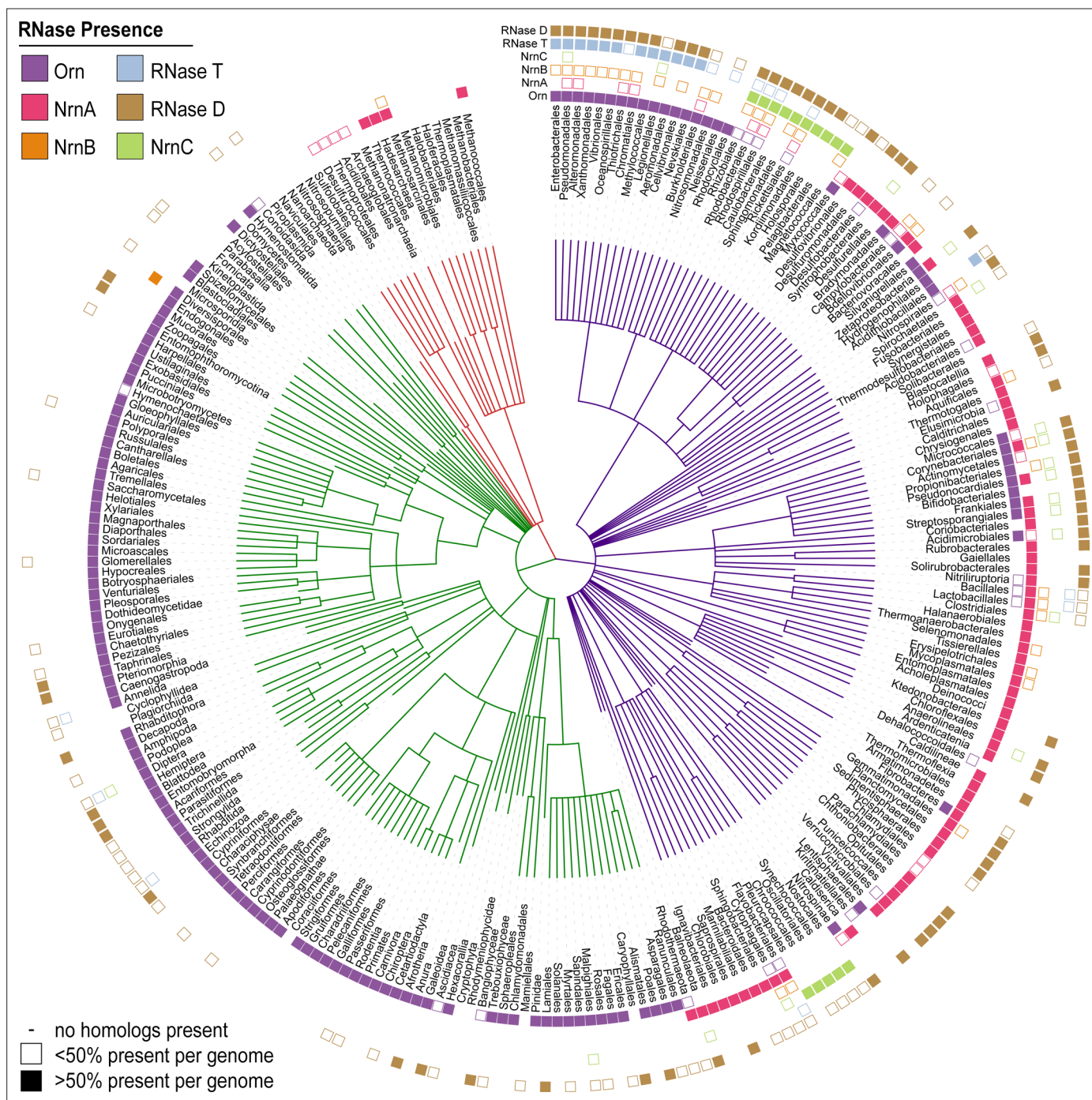


Figure 6. Presence of RNase homologs across sequenced organism classes. Shown is a ‘Tree of Life’ with all taxonomic groups at the class level with at least one substantially complete proteome available in the dataset. The tree is based on the structure of the NCBI Taxonomy database, with bacterial taxa shown with purple lines, eukaryotic taxa shown with green lines, and archaeal taxa shown with red lines. The presence of each RNase homolog as a proportion of the total proteins in that taxonomic group is shown as either a filled square (>50% presence of a homolog per genome) or an empty square (<50% presence of a homolog per genome). Lack of a square indicates no homologs for that family were present in genomes of that class.

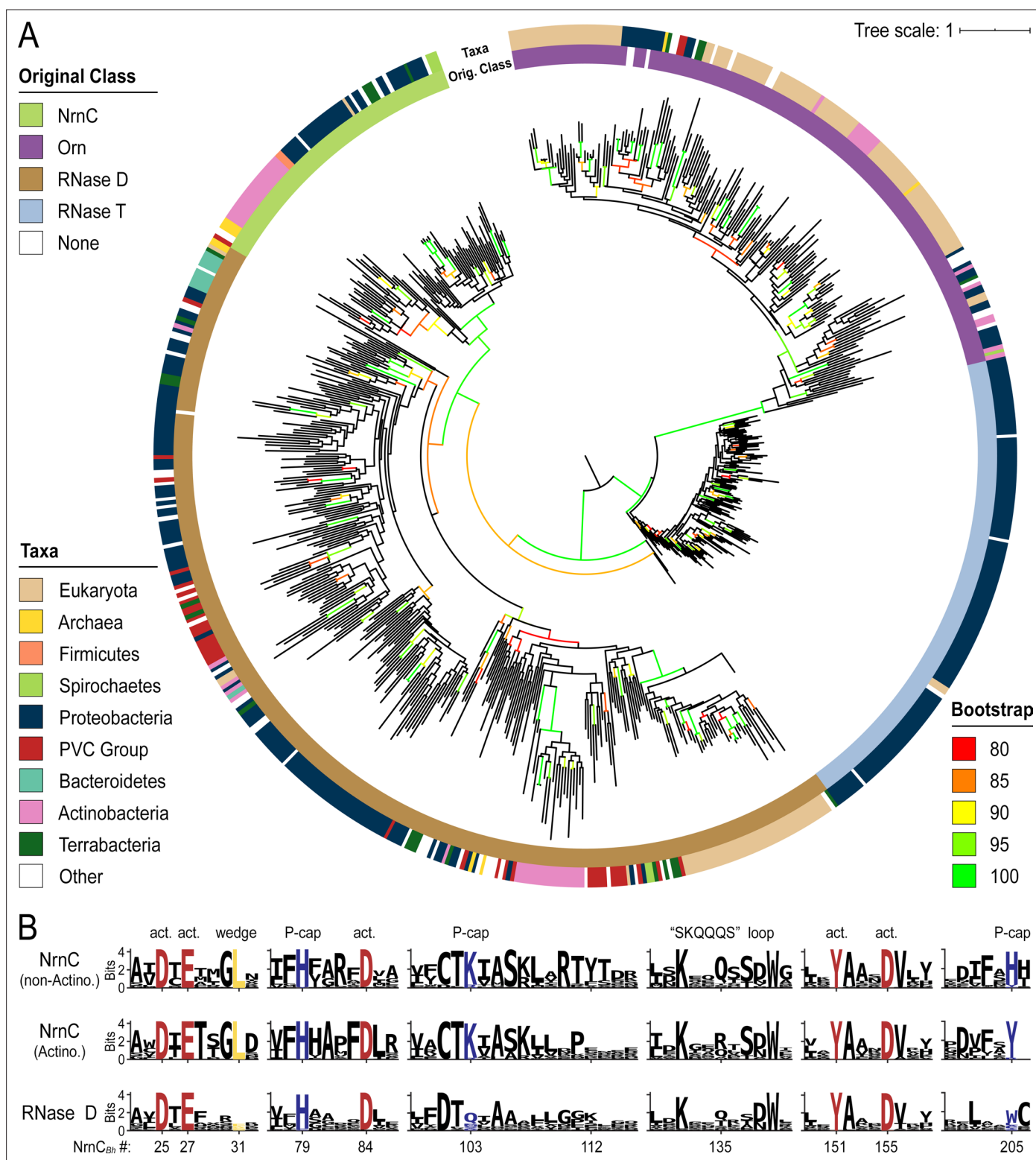


Figure 7. Phylogenetic tree of four DnaQ-fold RNase families. **(A)** Phylogenetic tree of 669 representatives of the RNase T, RNase D, oligoribonuclease (Orn), and nano-RNase C (NrnC) families of RNase proteins. The inner ring represents the original classification of each sequence by HMM analysis. The outer ring represents the high-level taxonomic classification of the organism the protein is found in. The color of the branch represents the UFBoot bootstrap value, where black branches are <80%, red is 80%, orange is 85%, yellow is 90%, light green is 95%, and bright green is 100%. Bootstrap values > 90% indicate high-confidence splits. **(B)** Sequence logos of RNase D and NrnC subgroups. Sequence logos showing the relative entropy (information content) at selected positions in RNase D as well as the Actinobacterial and non-Actinobacterial subsets of NrnC. Sequence numbering is relative to *Bartonella birtlessi* NrnC (G4VUY7). Active site residues are shown in red, phosphate cap residues in dark blue, and the L-wedge in yellow.

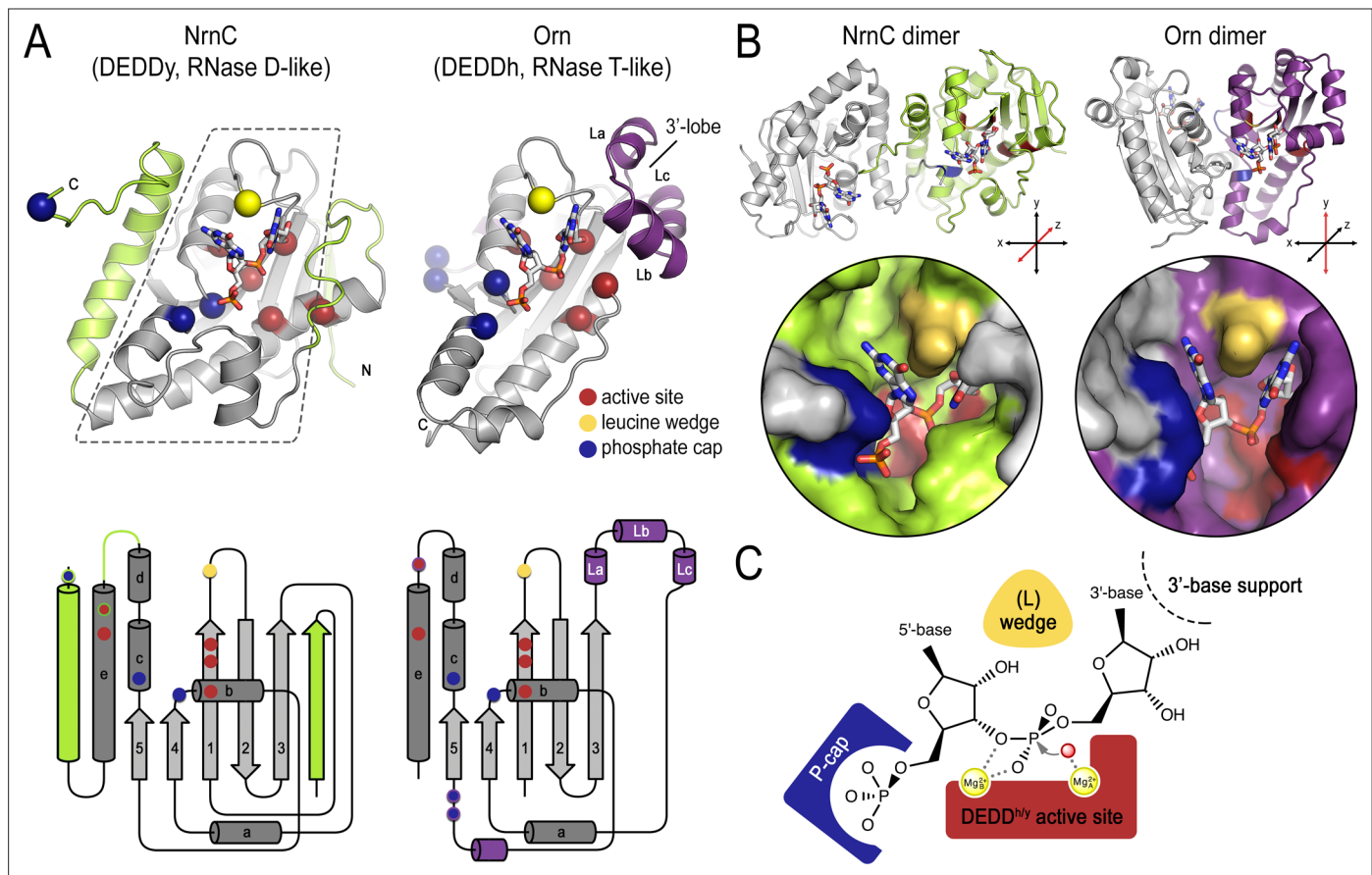


Figure 8. Structural comparison of nano-RNase C (NrnC) and oligoribonuclease (Orn). **(A)** Fold topology. pGG-bound NrnC and Orn monomers are shown in a similar orientation as cartoons (top) or schematic topology diagrams (bottom). Conserved catalytic core elements are colored in gray. NrnC and Orn-specific features are colored in green and purple, respectively. Other color codes mark the positions of the DEDDy/h motif (red spheres), L-wedge (yellow sphere), and phosphate cap residues (dark blue spheres). **(B)** Comparison of dimer units of NrnC and Orn (top) with close-ups of the composite active sites of the enzymes (bottom). An NrnC monomer is colored green and an Orn monomer is colored purple, with adjacent monomers in the biological assemblies colored in light gray. Specific residues are colored as in (A). Coordinate systems indicate the twofold symmetry axis of the enzyme dimers, with the colored monomers shown in a similar orientation. **(C)** Structurally and functionally conserved features common among NrnC- and Orn-type diribonucleases.